AGU PUBLICATIONS

Geophysical Research Letters

RESEARCH LETTER
10.1002/2017GL076229

Key Points:
- Inclusion of ocean geostrophic currents has an important impact on ice-ocean stress and therefore total ocean surface stress calculations
- The feedback of ocean circulation on ice-ocean stress and observed stress curl reversal stabilize the intensity of the Beaufort Gyre
- Changing dynamic ocean topography from upwelling or downwelling scenarios is one feedback pathway for stabilization from ice-ocean interaction

Correspondence to:
S. Dewey,
deweys@uw.edu

Citation:
Dewey, S., Morison, J., Kwok, R., Dickinson, S., Morison, D., & Andersen, R. (2018). Arctic ice-ocean coupling and gyre equilibration observed with remote sensing. *Geophysical Research Letters*, *45*, 1499–1508. https://doi.org/10.1002/2017GL076229

Received 30 OCT 2017
Accepted 17 JAN 2018
Accepted article online 24 JAN 2018
Published online 6 FEB 2018

Arctic Ice-Ocean Coupling and Gyre Equilibration Observed With Remote Sensing

Sarah Dewey[1,2], James Morison[1,2], Ronald Kwok[3], Suzanne Dickinson[2], David Morison[4], and Roger Andersen[2]

[1]School of Oceanography, University of Washington, Seattle, WA, USA, [2]Polar Science Center, Applied Physics Laboratory, University of Washington, Seattle, WA, USA, [3]Jet Propulsion Laboratory, Pasadena, CA, USA, [4]University of Utah, Salt Lake City, UT, USA

Abstract Model and observational evidence has shown that ocean current speeds in the Beaufort Gyre have increased and recently stabilized. Because these currents rival ice drift speeds, we examine the potential for the Beaufort Gyre's shift from a system in which the wind drives the ice and the ice drives a passive ocean to one in which the ocean often, in the absence of high winds, drives the ice. The resultant stress exerted on the ocean by the ice and the resultant Ekman pumping are reversed, without any change in average wind stress curl. Through these curl reversals, the ice-ocean stress provides a key feedback in Beaufort Gyre stabilization. This manuscript constitutes one of the first observational studies of ice-ocean stress inclusive of geostrophic ocean currents, by making use of recently available remote sensing data.

1. Background

The correspondence among wind, ice drift, and Arctic Ocean circulation has been studied since Nansen's observation that ice moves at 20° to the right of surface wind and at 2% of the wind speed (Nansen, 1902). Thorndike and Colony (1982, hereafter referred to as TC82) regress winds and buoy-derived ice velocity and confirm Nansen's rule of thumb with respect to the ice velocity's variance. This result can lead to the idealization that ice motion is solely dependent on wind (e.g., Ma et al., 2017). However, TC82 also find it impossible to distinguish the forcing of mean ice velocities between wind forced and ocean forced. Indeed, Arctic sea ice velocity shows a strong similarity to geostrophic ocean surface velocity from Ice, Cloud, and land Elevation Satellite (ICESat) dynamic ocean topography (DOT) in 2004–2009 (Morison et al., 2012), implying that ocean forcing plays a significant role in driving the ice.

Kwok et al. (2013) perform an updated regression analysis similar to TC82 but informed by present Arctic ice conditions and remote sensing data. The pattern of residual ice velocity that they attribute to the ocean strongly resembles the ocean velocity from ICESat DOT. Moreover, they find that for the most part ocean speeds exceed ice speeds, suggesting the ocean is driving the ice rather than acting as a passive drag on wind-driven motion.

The tendency for the ocean to drive the ice is apparent, and perhaps nowhere more important than, in the Beaufort Sea. The Beaufort Gyre is one of the dominant features of the mean Arctic Ocean circulation. Driven by the Beaufort High in atmospheric pressure, it flows anticyclonically over the Canada Basin and is a convergence zone boasting the highest sea surface height (Kwok & Morison, 2011) and freshwater content in the Arctic Ocean (Carmack et al., 2008; Serreze et al., 2006). Locally, this freshwater influences stratification and sea ice formation; were it to exit the Arctic Ocean, it could potentially disrupt deep water formation, the ocean's meridional overturning circulation, and global climate (Aagaard & Camack, 1989; Jahn & Holland, 2013; Koenigk et al., 2007; Proshutinsky & Johnson, 1997; Proshutinsky et al., 2002; Sévellec et al., 2017).

The Beaufort Sea has been identified as a region of the largest summer sea ice areal decline in the past decade (Comiso et al., 2008) and has experienced the greatest recent loss in multiyear sea ice (Maslanik et al., 2011). Given its role in freshwater storage and the rapidly diminishing ice cover, the Beaufort Gyre has garnered much attention as a nexus of change, especially with respect to its recent accumulation of momentum.

Proshutinsky and Johnson (1997) propose two regimes of Arctic Ocean circulation based on the strength of the sea surface height gradient driving the Beaufort Gyre. In the anticyclonic (cyclonic) phase, the gyre intensifies (weakens) as surface height gradients increase (decrease) due to enhanced (reduced) Ekman transport convergence driven by more (less) negative surface stress curl under a strengthened (weakened) Beaufort

High. Expanding on this notion, Proshutinsky et al. (2009) emphasize the role of the anticyclonic phase in accumulating freshwater, relating a maximum of freshwater accumulation to maximally negative wind stress curl.

In the mid-2000s the Beaufort Gyre intensified and accumulated freshwater (McPhee et al., 2009; Proshutinsky et al., 2009). The intensification was manifest in satellite altimetry measurements of increased doming of the gyre (Giles et al., 2012; Morison et al., 2012). Objective analysis of a broad collection of hydrography (Rabe et al., 2011) corroborates the accumulation of freshwater in the gyre, as does freshwater content estimated from the trends in satellite-derived sea surface height (Giles et al., 2012) and the difference between this height and ocean bottom pressure (Morison et al., 2012).

The doming of the Beaufort Gyre is driven by convergence of Ekman transport, or Ekman pumping, in which the rate of doming is related to negative surface stress curl. Under the persistent negative stress curl of the Beaufort High, doming should continue to increase. However, model and observational evidence has shown that since about 2009, the Beaufort Gyre has stabilized following the period of spin-up (Armitage et al., 2017; Krishfield et al., 2014; Petty et al., 2016; Zhang et al., 2016). Freshwater content of the Beaufort Gyre has seemingly plateaued (Krishfield et al., 2014; Zhang et al., 2016), indicating that despite its persistently anticyclonic wind forcing, the gyre is no longer accumulating more freshwater. One explanation for this equilibration of the gyre is horizontal eddy diffusion of momentum in the ocean (Manucharyan & Spall, 2016; Manucharyan et al., 2016). Eddy diffusion that exports freshwater and momentum tends to balance halocline deepening due to anticyclonic surface forcing and is thus a contributor to long-term stability. Were this the only stabilization mechanism, the ice velocity would always exceed geostrophic water velocity. Instead, the recent stabilization of the Beaufort Gyre has been associated with geostrophic water velocity exceeding ice velocity.

Similar to the finding of Kwok et al. (2013), as part of the Beaufort Gyre spin-up, McPhee (2013) and Armitage et al. (2017) show that geostrophic ocean currents in the Canada Basin have increased to rival and sometimes exceed ice drift speeds. It is the relative velocity of the ice and ocean that determines the strength and direction of ice-ocean surface stress. Therefore, we argue that in the presence of an ice cover with internal ice stress, which dissipatively retards ice motion, the difference in ice and ocean velocities is a key agent in the observed gyre stabilization because of changing ice-ocean stress (Kwok & Morison, 2017). Specifically, where the ice is slowed by internal ice stress and the ocean moves faster than the ice, the sign of the ice-ocean stress and the associated Ekman pumping are reversed, and the gyre dome decreases—even as the sign of average wind stress curl may predict convergence.

Several model studies have looked at the change in ocean surface stress under recent, increasingly ice-free conditions (Martin et al., 2016, 2014; Tsamados et al., 2014; Zhang et al., 2012). This paper constitutes a first observational evaluation of the Ekman pumping-internal ice stress dissipation and its influence on gyre stabilization. Key advances in this analysis are the use of satellite-derived geostrophic velocities in the calculation of ice-ocean stress, which previous studies (Ma et al., 2017; Petty et al., 2016; Timmermans et al., 2014; Yang, 2009) have neglected, and the finding that for present conditions the Ekman pumping ice-ocean stress dissipation is likely at least twice as great as ocean eddy dissipation of gyre energy.

2. Coupling of Ice and Ocean Velocity

To understand the fundamental connection between ice motion ($\vec{V}$) and geostrophic water velocity ($\vec{V}_g$), we consider the quasi-steady state horizontal force balance for sea ice with complex velocity $\vec{V} = u + iv$, draft D, surface ocean density ρ_0, and horizontal length scale L. As discussed in McPhee (1980, 1982), this balance is one between the Coriolis effect ($if\left(\vec{V} - \vec{V}_g\right)$), air-ice stress ($\vec{\tau}_{ai}$), ice-ocean stress ($\vec{\tau}_{io}$), and horizontal internal ice stress ($\vec{\tau}_{ii}$), a result of interaction of the ice floes:

$$if\left(\vec{V} - \vec{V}_g\right) = \frac{1}{\rho_0 D}\left(\vec{\tau}_{ai} - \vec{\tau}_{io}\right) - \frac{1}{\rho_0 L}\vec{\tau}_{ii} \tag{1}$$

$\vec{\tau}_{ai}$ is the forcing solely dependent on the square of wind velocity because wind speed is so much larger than typical ice velocities. For the purpose of scaling, $\vec{\tau}_{ii}$ is an idealized representation of internal ice stress. At horizontal scales where the force exerted by internal ice stress is comparable to that exerted by surface stresses, $\vec{\tau}_{ii}/L$ is comparable to $\vec{\tau}_{ai}/D$. It can be considered a dissipative force dependent on horizontal gradients in ice velocity and is difficult to measure directly.

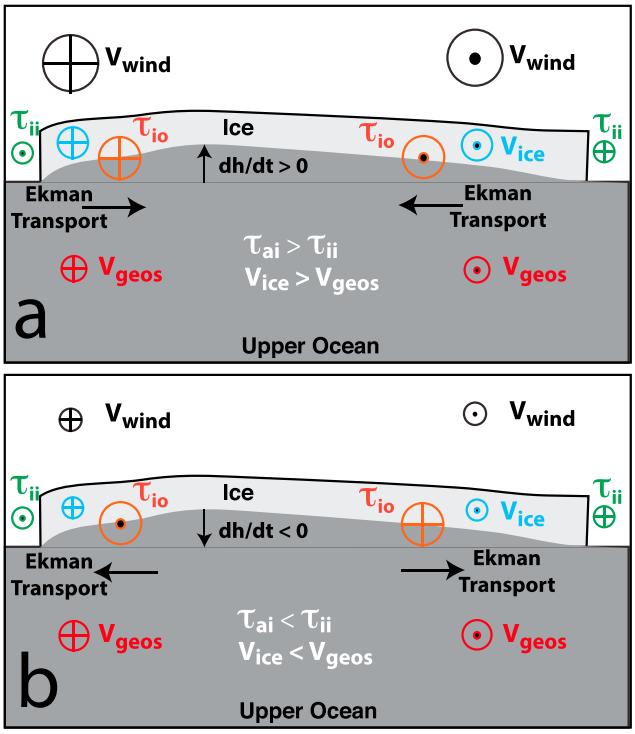

Figure 1. Illustration of Ekman pumping-internal stress feedback for gyre equilibration (adapted from Kwok & Morison, 2017). (top) The condition in which the wind stress dominates the internal ice stress, and ice velocity is greater than the surface geostrophic water velocity. In this case, Ekman convergence increases the surface tilt (doming) and this in turn increases the surface geostrophic velocity. (bottom) The condition in which internal ice stress is greater than the wind stress, and the surface geostrophic water velocity is greater than the ice velocity. In this case, the ice-ocean stress leads to divergence (less doming) and, with this decrease in tilt, decreases the ice and ocean geostrophic velocities.

$\vec{V}_g$ is the surface geostrophic water velocity forced by the horizontal gradient in DOT, η:

$$\vec{V}_g = u_g + iv_g = i\frac{g}{f}\left(\frac{\partial\eta}{\partial x} + i\frac{\partial\eta}{\partial y}\right) \tag{2}$$

$\vec{V}_g$ appears in (1) as an expression of the force exerted on the ice by the gradient in η. The ice-ocean stress, $\vec{\tau}_{io}$, is related by the quadratic geostrophic drag law to the difference between ice velocity and $\vec{V}_g$ (McPhee, 2008). Consequently, (1) indicates that whenever wind stress forcing is small and horizontal scales are large enough or the ice cover thin enough to reduce internal ice stress, sea ice velocities are damped to the geostrophic water velocity. This explains in part the similarity of large-scale ice velocity and Arctic Ocean surface circulation (Kwok et al., 2013). However, ice velocity is also coupled to the geostrophic water velocity (or sea surface tilt) indirectly through Ekman transport convergence (Ekman pumping):

$$W_{Ek} = \nabla\times\left(\frac{\tau}{\rho_0 f}\right) \tag{3}$$

$$\tau = \alpha\tau_{io} + (1-\alpha)\tau_{ao} \tag{4}$$

where W_{Ek} is the vertical velocity difference between the surface and the bottom of the ocean planetary boundary layer due to Ekman transport convergence, α is the ice concentration, and τ_{ao} is the wind stress on open water areas.

The relative degree to which W_{Ek} affects the surface height, η, and the isopycnals below the mixed layer depends on the time and space scales of the forcing. For Arctic latitudes at basin length scales and time scales shorter than seasonal to a year, the ocean response is largely barotropic (Vinogradova et al., 2007) so that much of W_{Ek} can result in vertical velocity of the surface, $\dot{\eta}$. At shorter space scales and longer time scales baroclinic adjustment occurs so that a larger fraction of W_{Ek} goes into displacing isopycnals. In any event, negative (positive) stress curl results in upward (downward) $\dot{\eta}$ and progressive doming (dishing) of the surface.

At lower latitudes where the beta effect (variation of f with latitude) is strong, the progressive change in the surface height and isopycnal depth is dissipated by generation of Rossby waves. In an ice-free Arctic Ocean, where beta is small and this dissipation mechanism is essentially unavailable, doming and pycnocline displacements would likely increase until limited by interaction with topography or baroclinic instability. However, under an ice cover this progressive doming is limited because it increases the associated geostrophic water velocity while internal ice stress retards ice velocity. This proceeds until the geostrophic water exceeds ice velocity so that ice-ocean stress, stress curl, and W_{Ek} reverse, doming stops, and Ekman pumping reverses (Figure 1) (Kwok & Morison, 2017) until ice velocity and the geostrophic water velocity equilibrate.

Ultimately, the Beaufort Gyre is subject to a three-way balance between spin-up, the Ekman pumping-internal ice stress feedback, and the generation of eddy flux (Meneghello et al., 2017) by baroclinic instability. Our observations indicate that with the present ice cover, the Ekman pumping-internal ice stress feedback contributes more to gyre stabilization than eddy flux.

3. Methods and Data

Using constitutive relationships for the total ice-ocean and air-ocean stresses (equations (5) and (6)), we then scale the stresses by interpolated ERA-Interim ice concentration (Yang, 2009) to yield surface stress at each point on a 25-km equal area polar stereographic grid (4). Here we refer to doming of the surface and downward motion of the pycnocline as downwelling and downward surface motion with upward motion of the

pycnocline as upwelling. The curl of τ is then used to diagnose downwelling (upwelling) or freshwater accumulation (release) conditions (equation (3)).

$$\vec{\tau}_{\mathrm{io}} = \rho_o |C_{iw}| e^{i\beta} \left(\vec{u}_i - \vec{u}_g\right) \left|\vec{u}_i - \vec{u}_g\right| \tag{5}$$

$$\vec{\tau}_{\mathrm{ao}} = C_d \rho_a \vec{U}_{10} \left|\vec{U}_{10}\right| \tag{6}$$

In these equations, ρ_o and ρ_a represent the surface densities of water and air, respectively. $\vec{u}_i$, $\vec{u}_g$, and $\vec{U}_{10}$ are the velocities of sea ice, ocean geostrophic surface velocity, and 10 m winds, respectively. C_d is an air-ocean drag coefficient, here taken as 1.25×10^{-3}. C_{iw} and β are the drag coefficient and the turning angle of the ocean geostrophic drag law for which we use the values of 5.5×10^{-3} and 23° (McPhee, 1980). With a changing ice cover, there has been much effort to update these values (Cole et al., 2017, 2014; McPhee, 2012; and Lu et al., 2011), though a brief sensitivity analysis of β showed negligible changes in the magnitude of W_{Ek}.

DOT, in meters, is calculated from the Synthetic Aperture Interferometric Radar Altimeter on the European Space Agency's CryoSat-2 satellite (Kwok & Morison, 2016). The DOT data used here are 2-month averages from April 2011 to April 2015, a period shown by the model of Zhang et al. (2016) and the DOT observations of Armitage et al. (2017) to be one of stabilization of the Beaufort Gyre. The data are kriged to a grid, smoothed with a 250 km diameter Gaussian filter per McAdoo et al. (2013), and their gradients used to calculate ocean geostrophic velocities. Ocean surface density is interpolated to each 25-km grid point from the Polar science center Hydrographic Climatology (PHC) (Steele et al., 2001), though results are not sensitive to this choice of climatology. Air density is taken as the canonical value of 1.25 kg m^{-3}.

We use monthly, optimally interpolated, satellite-derived ice velocities (as described in Kwok et al., 2013, with a per vector uncertainty of 2 cm s^{-1}). These agree with International Arctic Buoy Programme buoy-derived velocities (Rigor, personal communication 2017). The buoy-satellite hybrid velocities of the National Snow and Ice Data Center (Tschudi et al., 2016) were not used because they are lower than our velocities and buoy velocities (Sumata et al., 2014, 2015) and thus exaggerate any ocean velocity exceedance of ice velocity. Also, their hybridization creates artificial divergence in the velocity field (Szanyi et al., 2016).

Monthly 10 m wind velocities and sea ice concentration come from ERA-Interim reanalysis (Dee et al., 2011), optimal both for spatial resolution (nominally 0.75° × 0.75°) and agreement with observations (Lindsay et al., 2014).

4. Sea Ice and Geostrophic Ocean Velocities

Our observed DOT and derived geostrophic velocities confirm that the ocean rivals the sea ice in speed. In order to present areal or temporal averages, we define the Beaufort Gyre region as within the box shown in Figure 2. Taking the mean over the 5 year period (April/May 2011 to April/May 2015) at each 25-km grid point (Figure 2a) demonstrates the similarity of average ice and geostrophic ocean velocities. Two main flow patterns emerge based on position in the gyre. In the eastern Beaufort Gyre region, the ocean velocities are constrained to align with bathymetry and run parallel to the Canadian Archipelago while the ice has a component toward the gyre center. In the western portion of the Beaufort Gyre region, the ocean demonstrates energetic northwestward flow. This flow has a large impact on ice-ocean stress and Ekman pumping in the region.

The averages over the Beaufort Gyre region indicate that the time-average ice and surface geostrophic ocean speeds are nearly the same, ranging from 1 to 6 cm s^{-1} (Figure 2b), and that this speed agrees with the model-based findings of Zhang et al. (2016, see their Figure 8), which were 3–4 cm s^{-1} after 2008. The ice, however, demonstrates higher speed variance (Figure 2c), compared to an ocean whose speed is more constant, similar to TC82. The ice variance, along with ice speed, tends to peak in the winter (December–January), likely due to intense storm events. Storminess may have caused the strong peak in December 2014–January 2015, because it was an exceptionally windy winter according to the model results of Liu et al. (2015). In December 2012–January 2013, the high variance may be due to a more motile ice pack following an extreme summer concentration minimum (Parkinson & Comiso, 2013). Variance and speed peak to a lesser extent in the spring at the onset of the melt season (April–May and June–July) as the ice pack first starts to loosen.

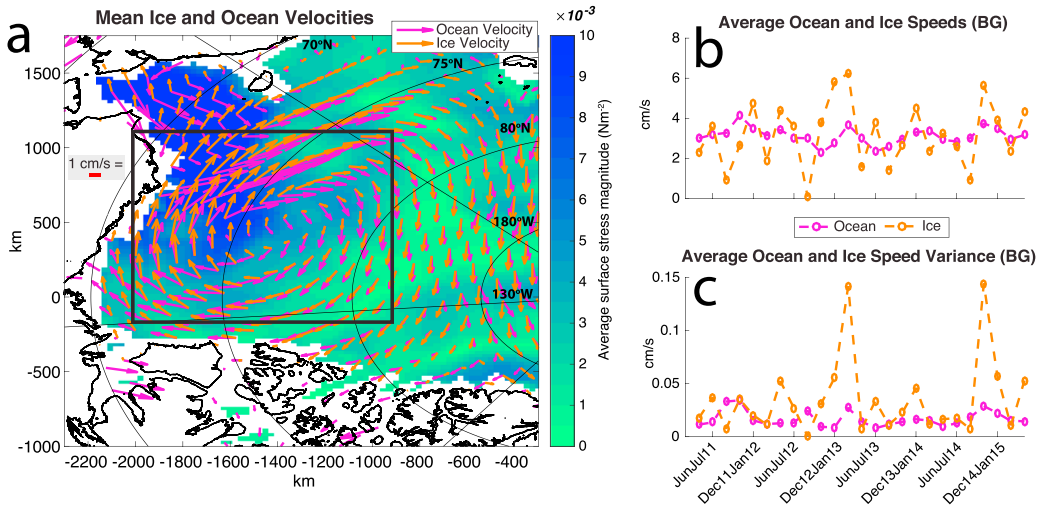

Figure 2. (a) Map of average ocean and ice velocity vectors over average surface stress magnitude. Ice velocities are only included in the calculation when ice is present. High stress magnitudes are centered in the western Beaufort Gyre, an area of particularly energetic ocean flow. (b and c) Time series of ice and ocean speeds and variance in the Beaufort Gyre region, as indicated by the box in Figure 2a. The ice and ocean move at comparable speeds, though the ice speed typically has more variance.

5. Ice-Ocean Feedback: Implications for Gyre Equilibration

The relative velocities of the ice and ocean determine which part of the ice-ocean system is exerting stress on the other. In a system where the ice and ocean are both moving anticyclonically, if the ice is moving faster than the ocean, downward Ekman pumping of the pycnocline and increased doming result. If the surface ocean is moving faster than the ice, the sign of the Ekman pumping reverses, the ocean surface flattens or dishes, and the system becomes an upwelling, divergent system (Figure 1).

The frequency with which the average Ekman pumping is of one sign or the other can indicate the stability of the gyre: If the gyre is convergent about half the time and divergent the other half, then we expect a stable system with a constant average upper-ocean freshwater content. Zhang et al. (2016) show that freshwater content in the Beaufort Gyre is fairly stable based on model output; Krishfield et al. (2014) observe the beginning of a freshwater content plateau in ice-tethered profile data. Raw data from Beaufort Gyre moorings show the same plateau through 2015 (Woods Hole Oceanographic Institution, 2017, see their Figure 3).

We use two measures of the frequency of divergence versus convergence. One is the spatially averaged value of Ekman pumping through time, and the other is the frequency with which ice-ocean stress opposes ocean motion (i.e., the swiftly flowing ocean is driving the ice). We consider the ocean to be driving the ice when the ocean speed exceeds ice speed and the ocean velocity vector is within 23° (β) of the ocean-to-ice (opposite of ice-to-ocean) stress vector. A map of the percentage of 2-month periods when the ocean drives the ice (Figure 3a) shows that for much of the Beaufort Gyre region, the ocean drives the ice about half the time. This is particularly true in the west near the Northwind Ridge region, in the northern part of the Beaufort Gyre, and along the margin of the Canadian Archipelago.

Considering $W_{\text{Ek-geos}}$ versus time (Figure 3b), we see that the Beaufort Gyre is an upwelling system about 40% of the time. There is a small seasonal signal when like months are averaged, with increased downwelling in the spring and fall and downwelling minima spaced 6–8 months apart, but this signal is overshadowed by other variations. With only the wind stress as forcing (that is, calculating $W_{\text{Ek-wind}}$ using only $C_d\rho_a\vec{U}_{10}|\vec{U}_{10}|$ and no ice-ocean stress), only two 2-month periods out of 25 demonstrate upwelling and there is even less variability in $W_{\text{Ek-wind}}$. Cumulatively integrating these quantities through time yields about 5 m of downwelling for $W_{\text{Ek-geos}}$, which, while negative, is a third of the value of $W_{\text{Ek-wind}}$ when only atmospheric forcing is considered. This difference suggests that the reversals in $W_{\text{Ek-geos}}$ bring the integral closer to the 0 value of a fully stabilized gyre.

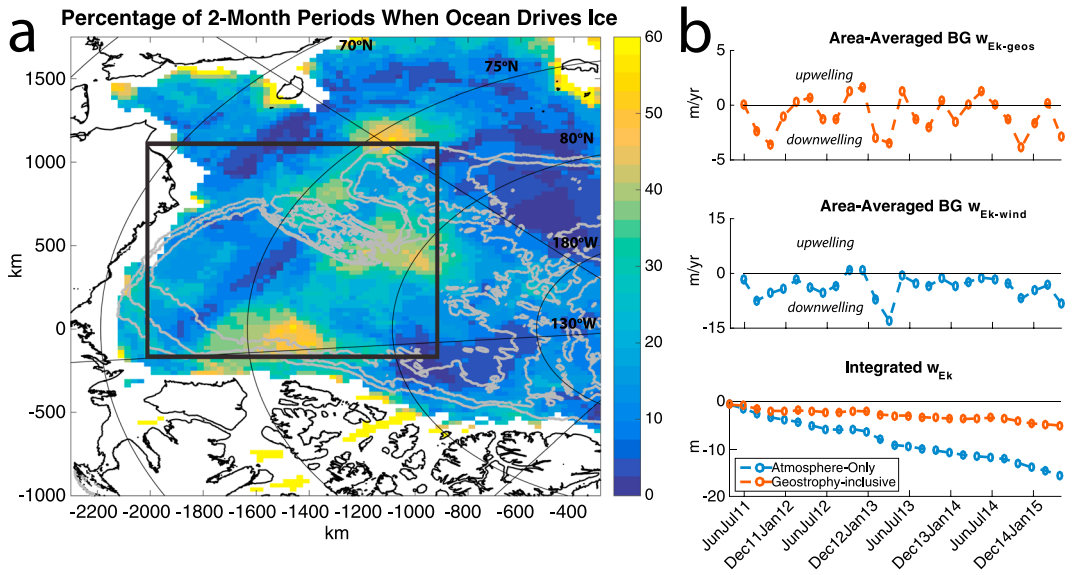

Figure 3. (a) Map of the frequency with which the ocean drives the ice. This parameter is calculated from how often the ocean speed exceeds the ice speed and ocean velocity vectors are pointed in the same direction (within $\beta = 23°$) as ocean-to-ice stress vectors. Within the Beaufort Gyre region, as indicated by the box, the ocean drives the ice between 20% and 60% of the time. (b) Time series of the Beaufort Gyre region average $W_{Ek\text{-}geos}$, as calculated within the box in Figure 3a. When geostrophic ocean velocity is included in the calculation, upwelling conditions prevail about 40% of the time, consistent with the frequency range shown in Figure 3a. When only the atmosphere is considered in the calculation of $W_{Ek\text{-}wind}$ (middle), the Beaufort Gyre switches to a consistently downwelling system. The order of magnitude of $W_{Ek\text{-}wind}$ is consistent with the 10–20 myr^{-1} downwelling rate reported by Timmermans et al. (2014). When each of these quantities is cumulatively integrated through time (bottom), the change in meters in the height of the geostrophic-inclusive scenario is one third that of the atmosphere-only case and closer to the 0 value that would indicate a stable gyre. In a stable gyre, this difference from 0 can be accounted for by the effects of other processes, such as horizontal eddy fluxes.

Additionally, the time series of $W_{Ek\text{-}geos}$ and geostrophic ocean velocities characterize the feedback that stabilizes the gyre. Take, for instance, the convergent scenario: With increased doming, we expect an increase in geostrophic ocean velocities (resulting from increased DOT) to lag slightly behind the peak of downwelling or negative $W_{Ek\text{-}geos}$. Indeed, when the time series of $W_{Ek\text{-}geos}$ and geostrophic ocean speed are considered, there is a significant negative correlation between the two ($r = -0.6$, $p < 0.01$) at a 2-month lag. The geostrophic ocean speed is not significantly autocorrelated beyond zero lag, so the $W_{Ek\text{-}geos}$-ocean speed relationship supports the proposed oceanic gyre equilibration mechanism. Thus, the time scale for this equilibration process is on the order of months (e.g., Dewey et al., 2017), not years. It is likely that this process has always been occurring, but our ability to observe it has been limited.

A question arising from this temporal analysis is whether the spatial distribution of $W_{Ek\text{-}geos}$ has any influence on stabilization. The Ekman pumping should be considered not only through time but also through space. A map of the average ocean surface stress curl from April–May 2011 to April–May 2015 shows some patchiness in downwelling and upwelling (Figure 4a)—patchiness not constrained to the Beaufort Gyre—indicating the potential for similar ice-ocean interaction to be occurring basin wide.

The presence or absence of sea ice hints at some of the reason for this patchiness. The sea ice concentration most conducive to stress curl reversals in the Beaufort Gyre is around 50%–80% (Figure 4b). Martin et al. (2014) point to the upper end of this concentration range as optimal for momentum transfer from air to ocean. Bordering the Canadian Archipelago, the ice concentration is higher and curl reversals more likely result from the differences in directions of ice and water velocities—even as average curl over the gyre may be negative, it may become positive locally where horizontal velocity shear occurs near land or less mobile ice. These conditions underscore the necessity of ice cover for stress curl reversal.

In the context of so much literature using wind stress curl as the determinant of Ekman pumping (e.g., Giles et al., 2012) and/or assuming zero ocean velocity (e.g., Petty et al., 2016; Timmermans et al., 2014), this

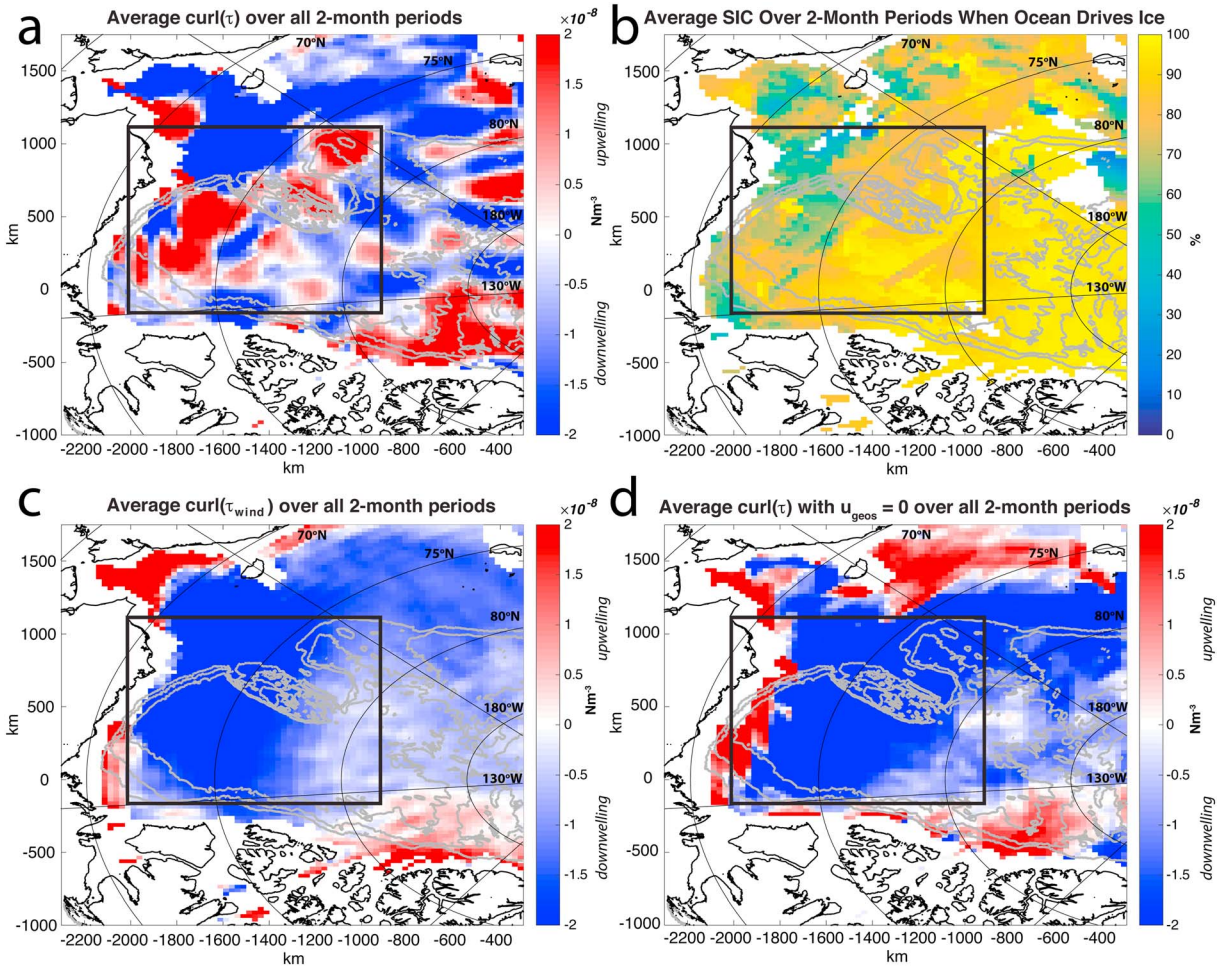

Figure 4. Maps showing (a) the average ocean surface stress curl over all months April/May 2011 to April/May 2015. The patchy nature of the curl map suggests interesting ice-ocean interaction outside of the immediate Beaufort Gyre. (b) Average sea ice cover over the periods when the ocean drives the ice (see Figure 3a for frequency map), and average ocean surface stress curl for the case studies of (c) wind-only forcing and (d) zero ocean geostrophic velocity.

calculation of ocean surface stress invites comparison with "atmosphere-only" and "zero ocean geostrophic current" scenarios. The degree to which the ocean surface stress in these cases differs from our earlier results demonstrates the importance of ice-ocean stress and nonzero geostrophic current. Atmosphere-only forcing (Figure 4c) and zero geostrophic current (Figure 4d) show the same pattern of upwelling adjacent to the coast with downwelling in the central Beaufort Gyre region. The scenario in which there is no geostrophic current has more coastal upwelling, indicating that the ice-ocean stress curl exceeds the theoretical atmosphere-ocean stress curl. This result is consistent with Spreen et al. (2011), who observe an increase in ice drift speed that cannot be accounted for by wind speed trends. They attribute much of this increase, especially in the near-coastal marginal seas, to thinner ice cover (i.e., wind momentum is converted into ice momentum more readily, with less internal ice stress).

6. Time Scales for Equilibration

Primarily because of the variability we see in Ekman pumping at bimonthly time scales (Figure 3a), our sense is that the Ekman pumping-ice drag stabilization has a time scale of days to 1 or 2 months. The data demonstrate variability at the 2-month interval inherent in our DOT averages. However, higher-frequency variability more likely comes from the atmosphere than the ocean. The time scale between major wind forcing events is about 2 to 3 weeks. The time scales of the physical processes are shorter still. The time scale of the Ekman pumping process is f^{-1} or about 12 h.

The inherent time scale for the decay of ice velocity due to horizontal shear in the ice (equation (1)) is $T = \frac{\rho L^2}{K_{\text{viscous}}}$, where K_{viscous} is the shear viscosity for an assumed viscous ice rheology. For a length scale, L = 200 km, corresponding to the scale beyond which surface forces have tended to dominate internal ice stress (TC82), and for K_{viscous} equal to 10^{10} kg m^{-1} s^{-1} (Leppäranta, 2005), T equals 1 h. At the low end of the viscosity range, with $K_{\text{viscous}} = 10^8$ kg m^{-1} s^{-1}, T equals about 4 days. These scales indicate Ekman pumping, and ice drag stabilize ice and ocean velocity at time scales of less than a week.

In contrast, gyre adjustment through eddy generation occurs with a time scale ($T \sim L^2/K_{\text{eddy}}$) of 6 years (Manucharyan & Spall, 2016). Observations suggest K_{eddy} = 500 m^2 s^{-1} (Meneghello et al., 2017), implying T = 3 years for L = 200 km. Carmack et al. (2008) estimate the ocean freshwater residence time in the Canada Basin to be 11 years, with the sea ice residence time closer to 3–5 years, suggesting similar time scales for leakage of mass and momentum from the gyre. These diffusion processes have time scales much longer than the Ekman pumping-ice drag feedback.

7. Conclusions

We have calculated ocean surface stress using DOT-derived geostrophic velocities, satellite-derived ice velocities, and reanalysis winds. Ocean geostrophic velocity in the Beaufort Gyre area rivals that of the overlying sea ice, and the ocean often drives the ice, leading to frequent surface stress curl reversals. With these reversals come changes in the ocean between upwelling and downwelling systems, leading to a gyre that is stable over time. We propose a feedback between the internal ice stress and the ocean geostrophic velocity, such that the relative influences of wind forcing and internal ice stress influence the doming of the ice and water and their velocities in turn (Figure 1).

Based on the fundamental force balance introduced in section 1, we think that this mechanism for gyre equilibration has been in place as long as there has been an ice cover in the Beaufort Gyre substantial enough to generate internal ice stress. Only recent advances in observations have allowed it to be measured. Among the different dissipation processes that may counteract wind-driven gyre spin-up, our proposed mechanism operates on daily to monthly scales. Consequently, the interplay of atmosphere, ice, and ocean has reached a critical point where the Beaufort Gyre is stable following years of spin-up. Geostrophic ocean currents rival ice motion and cannot be neglected.

Acknowledgments

This work was supported by the Office of Naval Research grant N00014-15-1-2295 and NASA grant NNX13AP72G. R. Kwok was supported by the National Aeronautics and Space Administration through a contract with the Jet Propulsion Laboratory, California Institute of Technology. CryoSat-2 DOT data are available from the European Space Agency at https://earth.esa.int/web/guest/missions/esa-operational-eo-missions/cryosat and from the Radar Altimeter Database System (RADS) at http://rads.tudelft.nl/rads/data/authentication.cgi; all other data sources are listed in the references. The authors thank Benjamin Rabe and one other anonymous reviewer for their insight and assistance in improving this manuscript.

References

Aagaard, K., & Camack, E. C. (1989). The role of sea ice and other fresh water in the Arctic circulation. *Journal of Geophysical Research*, *94*(C10), 14485. https://doi.org/10.1029/JC094iC10p14485

Armitage, T. W. K., Bacon, S., Ridout, A. L., Petty, A. A., Wolbach, S., & Tsamados, M. (2017). Arctic Ocean geostrophic circulation 2003–2014. *The Cryosphere Discussions*, 1–32. https://doi.org/10.5194/tc-2017-22

Carmack, E., McLaughlin, F., Yamamoto-Kawai, M., Itoh, M., Shimada, K., & Krishfield, R. (2008). Freshwater storage in the Northern Ocean and the special role of the Beaufort Gyre. In R. R. Dickson, J. Meincke, & P. B. Rhines (Eds.), *Arctic-subarctic ocean fluxes* (pp. 145–169). Dordrecht, Netherlands: Springer. https://doi.org/10.1007/978-1-4020-6774-7_8

Cole, S. T., Timmermans, M.-L., Toole, J. M., Krishfield, R. A., & Thwaites, F. T. (2014). Ekman veering, internal waves, and turbulence observed under Arctic sea ice. *Journal of Physical Oceanography*, *44*(5), 1306–1328. https://doi.org/10.1175/JPO-D-12-0191.1

Cole, S. T., Toole, J. M., Lele, R., Timmermans, M.-L., Gallaher, S. G., Stanton, T. P., … Thomson, J. (2017). Ice and ocean velocity in the Arctic marginal ice zone: Ice roughness and momentum transfer. *Elementa: Science of the Anthropocene*, *5*. https://doi.org/10.1525/elementa.241

Comiso, J. C., Parkinson, C. L., Gersten, R., & Stock, L. (2008). Accelerated decline in the Arctic sea ice cover. *Geophysical Research Letters*, *35*, L01703. https://doi.org/10.1029/2007GL031972

Dee, D. P., Uppala, S. M., Simmons, A. J., Berrisford, P., Poli, P., Kobayashi, S., … Vitart, F. (2011). The ERA-interim reanalysis: Configuration and performance of the data assimilation system. *Quarterly Journal of the Royal Meteorological Society*, *137*(656), 553–597. https://doi.org/10.1002/qj.828

Dewey, S. R., Morison, J. H., & Zhang, J. (2017). An edge-referenced surface fresh layer in the Beaufort Sea seasonal ice zone. *Journal of Physical Oceanography*, *47*(5), 1125–1144. https://doi.org/10.1175/JPO-D-16-0158.1

Giles, K. A., Laxon, S. W., Ridout, A. L., Wingham, D. J., & Bacon, S. (2012). Western Arctic Ocean freshwater storage increased by wind-driven spin-up of the Beaufort Gyre. *Nature Geoscience*, *5*(3), 194–197. https://doi.org/10.1038/ngeo1379

Jahn, A., & Holland, M. M. (2013). Implications of Arctic sea ice changes for North Atlantic deep convection and the meridional overturning circulation in CCSM4-CMIP5 simulations: MOC impacts of Arctic changes. *Geophysical Research Letters*, *40*, 1206–1211. https://doi.org/10.1002/grl.50183

Koenigk, T., Mikolajewicz, U., Haak, H., & Jungclaus, J. (2007). Arctic freshwater export in the 20th and 21st centuries: Arctic freshwater export from 1900 to 2100. *Journal of Geophysical Research*, *112*, G04S41. https://doi.org/10.1029/2006JG000274

Krishfield, R. A., Proshutinsky, A., Tateyama, K., Williams, W. J., Carmack, E. C., McLaughlin, F. A., & Timmermans, M.-L. (2014). Deterioration of perennial sea ice in the Beaufort Gyre from 2003 to 2012 and its impact on the oceanic freshwater cycle: Sea ice in the BG from 2003 to 2012. *Journal of Geophysical Research: Oceans*, *119*, 1271–1305. https://doi.org/10.1002/2013JC008999

Kwok, R., & Morison, J. (2011). Dynamic topography of the ice-covered Arctic Ocean from ICESat: Dynamic Topography of Arctic Ocean. *Geophysical Research Letters*, *38*, L02501. https://doi.org/10.1029/2010GL046063

Kwok, R., & Morison, J. (2016). Sea surface height and dynamic topography of the ice-covered oceans from CryoSat-2: 2011-2014: Sea surface height of ice-covered oceans. *Journal of Geophysical Research: Oceans*, *121*, 674–692. https://doi.org/10.1002/2015JC011357

Kwok, R., & Morison, J. (2017). Recent changes in Arctic sea ice and ocean circulation. *US CLIVAR Variations (Summer 2017)*, *15*(3), 1–6.

Kwok, R., Spreen, G., & Pang, S. (2013). Arctic sea ice circulation and drift speed: Decadal trends and ocean currents: Arctic sea ice motion. *Journal of Geophysical Research: Oceans*, *118*, 2408–2425. https://doi.org/10.1002/jgrc.20191

Leppäranta, M. (2005). *The drift of sea ice, springer-praxis books in geophysical sciences*. Berlin; New York: Chichester, UK: Springer; Praxis.

Lindsay, R., Wensnahan, M., Schweiger, A., & Zhang, J. (2014). Evaluation of seven different atmospheric reanalysis products in the Arctic*. *Journal of Climate*, *27*(7), 2588–2606. https://doi.org/10.1175/JCLI-D-13-00014.1

Liu, Z., Schweiger, A., & Lindsay, R. (2015). Observations and modeling of atmospheric profiles in the Arctic seasonal ice zone. *Monthly Weather Review*, *143*(1), 39–53. https://doi.org/10.1175/MWR-D-14-00118.1

Lu, P., Li, Z., Cheng, B., & Leppäranta, M. (2011). A parameterization of the ice-ocean drag coefficient. *Journal of Geophysical Research*, *116*, C07019. https://doi.org/10.1029/2010JC006878

Ma, B., Steele, M., & Lee, C. M. (2017). Ekman circulation in the Arctic Ocean: Beyond the Beaufort Gyre: Ekman circulation in the Arctic Ocean. *Journal of Geophysical Research: Oceans*, *122*, 3358–3374. https://doi.org/10.1002/2016JC012624

Manucharyan, G. E., & Spall, M. A. (2016). Wind-driven freshwater buildup and release in the Beaufort gyre constrained by mesoscale eddies: Eddy constrained Beaufort Gyre. *Geophysical Research Letters*, *43*, 273–282. https://doi.org/10.1002/2015GL065957

Manucharyan, G. E., Spall, M. A., & Thompson, A. F. (2016). A theory of the wind-driven Beaufort Gyre variability. *Journal of Physical Oceanography*, *46*(11), 3263–3278. https://doi.org/10.1175/JPO-D-16-0091.1

Martin, T., Steele, M., & Zhang, J. (2014). Seasonality and long-term trend of Arctic Ocean surface stress in a model. *Journal of Geophysical Research: Oceans*, *119*, 1723–1738. https://doi.org/10.1002/2013JC009425

Martin, T., Tsamados, M., Schroeder, D., & Feltham, D. L. (2016). The impact of variable sea ice roughness on changes in Arctic Ocean surface stress: A model study: Arctic Ocean surface stress. *Journal of Geophysical Research: Oceans*, *121*, 1931–1952. https://doi.org/10.1002/2015JC011186

Maslanik, J., Stroeve, J., Fowler, C., & Emery, W. (2011). Distribution and trends in Arctic sea ice age through spring 2011: Trends in Arctic sea ice age. *Geophysical Research Letters*, *38*, L13502. https://doi.org/10.1029/2011GL047735

McAdoo, D. C., Farrell, S. L., Laxon, S., Ridout, A., Zwally, H. J., & Yi, D. (2013). Gravity of the Arctic Ocean from satellite data with validations using airborne gravimetry: Oceanographic implications. *Journal of Geophysical Research: Oceans*, *118*, 917–930. https://doi.org/10.1002/jgrc.20080

McPhee, M. G. (1980). An analysis of pack ice drift in summer. In R. Pritchard (Ed.), *Sea ice processes and models* (pp. 62–75). Seattle: University of Washington Press.

McPhee, M. G. (1982). Sea ice drag laws and simple boundary layer concepts, including application to rapid melting.

McPhee, M. G. (2008). *Air-ice-ocean interaction: Turbulent ocean boundary layer exchange processes* (p. 215). Springer. https://doi.org/10.1007/978-0-387-78335-2

McPhee, M. G. (2012). Advances in understanding ice–ocean stress during and since AIDJEX. *Cold Regions Science and Technology*, *76-77*, 24–36. https://doi.org/10.1016/j.coldregions.2011.05.001

McPhee, M. G. (2013). Intensification of geostrophic currents in the Canada Basin, Arctic Ocean. *Journal of Climate*, *26*(10), 3130–3138. https://doi.org/10.1175/JCLI-D-12-00289.1

McPhee, M. G., Proshutinsky, A., Morison, J. H., Steele, M., & Alkire, M. B. (2009). Rapid change in freshwater content of the Arctic Ocean. *Geophysical Research Letters*, *36*, L10602. https://doi.org/10.1029/2009GL037525

Meneghello, G., Marshall, J., Cole, S. T., & Timmermans, M.-L. (2017). Observational inferences of lateral eddy diffusivity in the halocline of the Beaufort Gyre: Eddy diffusivity in the Beaufort Gyre. *Geophysical Research Letters*, *44*, 12,331–12,338. https://doi.org/10.1002/2017GL075126

Morison, J., Kwok, R., Peralta-Ferriz, C., Alkire, M., Rigor, I., Andersen, R., & Steele, M. (2012). Changing Arctic Ocean freshwater pathways. *Nature*, *481*(7379), 66–70. https://doi.org/10.1038/nature10705

Nansen, F. (1902). The oceanography of the North Polar Basin, *Rep*., 1–427 pp.

Parkinson, C. L., & Comiso, J. C. (2013). On the 2012 record low Arctic sea ice cover: Combined impact of preconditioning and an August storm: 2012 record low Arctic sea ice cover. *Geophysical Research Letters*, *40*, 1356–1361. https://doi.org/10.1002/grl.50349

Petty, A. A., Hutchings, J. K., Richter-Menge, J. A., & Tschudi, M. A. (2016). Sea ice circulation Around the Beaufort Gyre: The changing role of wind forcing and the sea ice state: Beaufort Gyre ice circulation. *Journal of Geophysical Research: Oceans*, *121*, 3278–3296. https://doi.org/10.1002/2015JC010903

Proshutinsky, A., Bourke, R. H., & McLaughlin, F. A. (2002). The role of the Beaufort Gyre in Arctic climate variability: Seasonal to decadal climate scales: Beaufort Gyre. *Geophysical Research Letters*, *29*(23), 2100. https://doi.org/10.1029/2002GL015847

Proshutinsky, A., Krishfield, R., Timmermans, M.-L., Toole, J., Carmack, E., McLaughlin, F., … Shimada, K. (2009). Beaufort gyre freshwater reservoir: State and variability from observations. *Journal of Geophysical Research*, *114*, C00A10. https://doi.org/10.1029/2008JC005104

Proshutinsky, A. Y., & Johnson, M. A. (1997). Two circulation regimes of the wind-driven Arctic Ocean. *Journal of Geophysical Research*, *102*(C6), 12,493–12,514. https://doi.org/10.1029/97JC00738

Rabe, B., Karcher, M., Schauer, U., Toole, J. M., Krishfield, R. A., Pisarev, S., … Kikuchi, T. (2011). An assessment of Arctic Ocean freshwater content changes from the 1990s to the 2006–2008 period. *Deep Sea Research Part I: Oceanographic Research Papers*, *58*(2), 173–185. https://doi.org/10.1016/j.dsr.2010.12.002

Serreze, M. C., Barrett, A. P., Slater, A. G., Woodgate, R. A., Aagaard, K., Lammers, R. B., … Lee, C. M. (2006). The large-scale freshwater cycle of the Arctic. *Journal of Geophysical Research*, *111*, C11010. https://doi.org/10.1029/2005JC003424

Sévellec, F., Fedorov, A. V., & Liu, W. (2017). Arctic sea-ice decline weakens the Atlantic meridional overturning circulation. *Nature Climate Change*, *7*(8), 604–610. https://doi.org/10.1038/nclimate3353

Spreen, G., Kwok, R., & Menemenlis, D. (2011). Trends in Arctic sea ice drift and role of wind forcing: 1992–2009: Trends in Arctic sea ice drift and wind. *Geophysical Research Letters*, *38*, L19501. https://doi.org/10.1029/2011GL048970

Steele, M., Morley, R., & Ermold, W. (2001). PHC: A global ocean hydrography with a high-quality Arctic Ocean. *Journal of Climate*, *14*(9), 2079–2087. https://doi.org/10.1175/1520-0442(2001)014,2079:PAGOHW.2.0.CO;2

Strong, C., & Rigor, I. G. (2013). Arctic marginal ice zone trending wider in summer and narrower in winter: Marginal ice zone trends. *Geophysical Research Letters*, *40*, 4864–4868. https://doi.org/10.1002/grl.50928

Sumata, H., Kwok, R., Gerdes, R., Kauker, F., & Karcher, M. (2015). Uncertainty of Arctic summer ice drift assessed by high-resolution SAR data: Uncertainty of Arctic summer ice drift. *Journal of Geophysical Research: Oceans*, *120*, 5285–5301. https://doi.org/10.1002/2015JC010810

Sumata, H., Lavergne, T., Girard-Ardhuin, F., Kimura, N., Tschudi, M. A., Kauker, F., … Gerdes, R. (2014). An intercomparison of Arctic ice drift products to deduce uncertainty estimates. *Journal of Geophysical Research: Oceans*, *119*, 4887–4921. https://doi.org/10.1002/2013JC009724

Szanyi, S., Lukovich, J. V., Barber, D. G., & Haller, G. (2016). Persistent artifacts in the NSIDC ice motion data set and their implications for analysis: Persistent artifacts in NSIDC ice drift. *Geophysical Research Letters*, *43*, 10,800–10,807. https://doi.org/10.1002/2016GL069799

Thorndike, A. S., & Colony, R. (1982). Sea ice motion in response to geostrophic winds. *Journal of Geophysical Research*, *87*(C8), 5845. https://doi.org/10.1029/JC087iC08p05845

Timmermans, M.-L., Proshutinsky, A., Golubeva, E., Jackson, J. M., Krishfield, R., McCall, M., … Nishino, S. (2014). Mechanisms of Pacific summer water variability in the Arctic's Central Canada Basin. *Journal of Geophysical Research: Oceans*, *119*, 7523–7548. https://doi.org/10.1002/2014JC010273

Tsamados, M., Feltham, D. L., Schroeder, D., Flocco, D., Farrell, S. L., Kurtz, N., … Bacon, S. (2014). Impact of variable atmospheric and oceanic form drag on simulations of Arctic Sea ice*. *Journal of Physical Oceanography*, *44*(5), 1329–1353. https://doi.org/10.1175/JPO-D-13-0215.1

Tschudi, M., Fowler, C., Maslanik, J., Stewart, J. S., & Meier, W. (2016). Polar Pathfinder daily 25 km EASE-Grid sea ice motion vectors. Version 3. Boulder, CO: National Snow and Ice Data Center. https://doi.org/10.5067/O57VAIT2AYYY

Vinogradova, N. T., Ponte, R. M., & Stammer, D. (2007). Relation between sea level and bottom pressure and the vertical dependence of oceanic variability. *Geophysical Research Letters*, *34*, L03608. https://doi.org/10.1029/2006GL028588

Woods Hole Oceanographic Institution (2017). Beaufort Gyre exploration project: BG freshwater content (FWC) reaches absolute maximum in 2015. Retrieved from http://www.whoi.edu/page.do?pid=153276, accessed online 10 October 2017

Yang, J. (2009). Seasonal and interannual variability of downwelling in the Beaufort Sea. *Journal of Geophysical Research*, *114*, C00A14. https://doi.org/10.1029/2008JC005084

Zhang, J., Lindsay, R., Schweiger, A., & Rigor, I. (2012). Recent changes in the dynamic properties of declining Arctic sea ice: A model study: Changes is sea ice dynamics. *Geophysical Research Letters*, *39*, L20503. https://doi.org/10.1029/2012GL053545

Zhang, J., Steele, M., Runciman, K., Dewey, S., Morison, J., Lee, C., … Toole, J. (2016). The Beaufort gyre intensification and stabilization: A model-observation synthesis: Beaufort Gyre stabilization. *Journal of Geophysical Research: Oceans*, *121*, 7933–7952. https://doi.org/10.1002/2016JC012196